



**HAL**  
open science

## Impact of external static electric field on surface tension of model solutions

Adrien Garcia, Tzvetelin Dessev, Luc Guihard, Sylvie Swyngedau Chevallier, Michel Havet, Alain Le-Bail

► **To cite this version:**

Adrien Garcia, Tzvetelin Dessev, Luc Guihard, Sylvie Swyngedau Chevallier, Michel Havet, et al.. Impact of external static electric field on surface tension of model solutions. *Innovative Food Science & Emerging Technologies / Innovative Food Science and Emerging Technologies*, 2023, 87, pp.103406. 10.1016/j.ifset.2023.103406 . hal-04147599

**HAL Id: hal-04147599**

**<https://hal.science/hal-04147599v1>**

Submitted on 30 Jun 2023

**HAL** is a multi-disciplinary open access archive for the deposit and dissemination of scientific research documents, whether they are published or not. The documents may come from teaching and research institutions in France or abroad, or from public or private research centers.

L'archive ouverte pluridisciplinaire **HAL**, est destinée au dépôt et à la diffusion de documents scientifiques de niveau recherche, publiés ou non, émanant des établissements d'enseignement et de recherche français ou étrangers, des laboratoires publics ou privés.

## Impact of external static electric field on surface tension of model solutions

Adrien Garcia<sup>(1)</sup>, Tzvetelin Dessev<sup>(2)</sup>, Luc Guihard<sup>(1)</sup>, Sylvie Swyngedau Chevallier<sup>(1)</sup>, Michel Havet<sup>(1,a)</sup>, Alain Le-Bail<sup>(1)</sup>

(1) ONIRIS, Nantes Université, CNRS, GEPEA, UMR 6144, Nantes, F-44000, France

(2) Nofima Mat, Food and Health Department, As 1430, Norway

(a) [michel.havet@oniris-nantes.fr](mailto:michel.havet@oniris-nantes.fr)

### HIGHLIGHTS

- Tensiometer measures liquid droplets surface tension under electric field.
- 3 model solutions used: water, WPI solution, and chickpea aquafaba.
- For protein solutions, significant reduction of surface tension was determined.

### KEYWORDS

Surface tension reduction, static electric field, pendant droplet tensiometer, Laplace equations, image analysis

### ABSTRACT

Food foams are thermodynamically unstable systems. Their stabilization remains a challenge in the industry. To understand the interactions between an electrostatic field (SEF) and food foam, a microscopic study was conducted. Using a specially designed tensiometer, a liquid droplet (water, WPI solution, chickpea liquor) was placed between two parallel electrodes and subjected to an SEF (0 to 800 kV/m). Images of the pendant droplet were recorded throughout the experiment. Based on Laplace's equation, the surface tension was calculated as function of the applied voltage.

The geometry of the droplet was deformed under SEF. The surface tension decreased proportionally to the rise of the voltage ( $\gamma_{distilled\ water} = 21.7 \cdot 10^{-3} \text{ N/m}$  at 800 kV/m).

The mechanism causing surface tension reduction was found to be the electric charge existing on the liquid surface. By reducing surface tension, drops are likely to break up more easily during expansion, which improves the organoleptic qualities of the foam.

## 27 1. INTRODUCTION

28 Aerated products represent a major part of the products processed by the food industry. They  
29 can be found in almost all kinds of food categories in a wide variety of forms: bread, beer foam,  
30 dessert foams, ice cream, etc. A food foam is defined as a biphasic structure in which one of  
31 the two phases, the gas in this case, is dispersed in variable diameter bubbles in a continuous  
32 phase which may be liquid, semi-solid or solid (Talansier et al., 2012).

33 Although food foams are now widely available, their production, and especially their  
34 stabilisation over time, remains a challenge for manufacturers. Foams are thermodynamically  
35 unstable objects. The smaller gas bubbles in the continuous phase will naturally seek to merge  
36 with each other to form larger bubbles in order to lower their internal pressure (Schramm 2006).  
37 The liquid phase will tend to separate from the gas phase by migrating downwards in the  
38 product, under the effect of gravity (Audebert 2018; Boissonnet 1998). The destabilization  
39 mechanisms are numerous but they are all linked to the same phenomenon, namely an excess  
40 of surface tension at the gas/liquid interfaces.

41 The "surface tension" (ST) is linked to an attractive intermolecular force associated to the  
42 cohesion of the molecules. In terms of energy, the surface tension can be seen as the energy  
43 required per unit area to create an interface between two immiscible materials - fluids or solids.  
44 According to Castellanos (1998), an increase in surface area  $\Delta A$  requires work  $W$  such that:

$$45 \qquad W = \sigma \cdot \Delta A \qquad (1)$$

46 ➤ with  $\sigma$ , surface tension (N.m-1)

47 Numerous studies demonstrated the importance of lowering ST to promote foam expansion  
48 (Nicorescu 2009). Today, manufacturers use energy-intensive mixers to generate foams with  
49 small bubbles; the use of surfactants is often considered to lower the surface tension. However,  
50 extrapolating the work done on dielectric materials to food matrices, foam generation, coupled  
51 with the use of a static electric field (SEF), appears to be an innovative method that would  
52 enable to durably stabilize a foam, by limiting the use of additives in the formulation, while  
53 reducing the energy consumption and the viscous dissipation (heatup) during processing.

54 In the field of thermal processes and heat transfer, Siedel (2012) performed boiling  
55 experiments in the presence of  $50 \text{ kV.cm}^{-1}$  electric fields, and the effect of SEF on heat transfer  
56 and bubble dynamics was characterized. The modification of the convective structures by the  
57 presence of SEF was described, showing smaller convective cells and more intense convective

58 activity. The consequent enhancement of heat transfer was quantified showing that the vapour  
59 production rate is decreased during bubble growth. The electrohydrodynamic effects on bubble  
60 dynamics was investigated showing that the bubble growth curve was modified but there is no  
61 clear influence of the SEF concerning the bubble departing frequency and the volume at  
62 departure. Although the volume of the bubbles at detachment and the relationship between the  
63 bubble frequency and the wall superheat were not affected, the bubble growth curve was  
64 modified. Siedel observed that bubbles were elongated in the direction of the SEF. The rising  
65 velocity of the bubble was also reduced in the presence of SEF, and the behaviour of bubbles  
66 growing side by side was modified, the SEF causing the bubbles to repel each other. These  
67 results provide compelling evidence that SEF can alter the bubble dynamics and subsequently  
68 heat transfer rates during boiling of dielectric fluids.

69 By focussing on the atomisation process, Sato et al. (1997) showed that the applied SEF  
70 enhanced atomisation because it was responsible for the decrease of the average diameter of  
71 formed droplets, due to ST reduction. Reduction of ST due to the applied voltage was  
72 proportional to the square of the voltage. The reduction varied with the electrical conductivity  
73 of the liquid and when the electrical conductivity  $> 10^2 \text{ S.m}^{-1}$ , the measured reduction was in  
74 good agreement with theory.

75 However, in the fields of chemical foams, Bonhomme et al. (2020) showed that applying an  
76 external SEF at the edge of the foam induces some liquid flows and, depending on the flow  
77 magnitude, it controls either gravity driven drainage, the foam stability, or the foam collapse at  
78 a specific location. While the liquid fraction of a foam tends to decrease as a function of foam  
79 height and time, at certain very specific values of capillary number and SEF, there is a reversal  
80 of the trend: the application of an SEF can therefore reverse the drainage.

81 The dynamics of droplet formation under the influence of an external SEF have been also  
82 studied by numerical investigation (Notz and Basaran 1999; Borthakur, Biswas, and  
83 Bandyopadhyay 2018). The studies were mostly carried out by solving axisymmetric  
84 electrohydrodynamic equations. The studies revealed that under the influence of an SEF,  
85 prolate-shaped droplets are formed at the orifice in the case of perfect dielectric fluids. The  
86 applied SEF strength and the ratio of the dielectric permittivity of the fluids play a pivotal role  
87 in deciding the magnitude of deformation as well as the volume of the droplets. The local SEF  
88 intensity inside the droplet is significantly altered due to the permittivity contrast between the  
89 fluids. The computations for leaky dielectric fluids reveal that both prolate - and oblate - shaped

90 droplets can be formed depending on the combination of the fluid conductivity and permittivity  
91 ratios (Borthakur, Biswas, and Bandyopadhyay 2018). The breakup time and detached droplet  
92 volume can be suitably tuned by varying the strength of the applied SEF.

93 All these elements suggest that generating a foam under a SEF would have an influence on the  
94 gas/liquid interface that constitutes each bubble contained in the foam. If the SEF reduces the  
95 surface tension, then the generation of small diameter bubbles would be facilitated with a lower  
96 energy consumption with an enhanced thermodynamic stability.

97 This paper presents the experiments carried out to validate these hypotheses. The authors have  
98 chosen to work at the scale of a droplet of liquid, generated with a pendant droplet tensiometer  
99 (Felix et al. 2021), from a protein solution, modelling a food matrix. The mechanisms that  
100 govern the stability of a foam take place at the gas/liquid interfaces. Therefore, the study of a  
101 liquid droplet in a gaseous environment allows a simple study of the mechanisms at the  
102 interfaces. While we have worked on liquid droplets for experimental convenience, the  
103 observations and results obtained could easily be transposed to gas bubbles (the case of food  
104 foams), because the real object of study is the gas/liquid interface. Using Laplace's equation  
105 and image analysis, the ST was calculated as a function of the applied tension. The novelty of  
106 this work lies in the experimentation on non-insulating matrices, such as food matrices.

## 107 **2. MATERIAL & METHODS**

### 108 **2.1. Model solutions**

109 To study the impact of the SEF at the scale of a droplet of liquid, three model solutions were  
110 selected. Distilled water was first considered as a control solution. Indeed, the value of the  
111 surface tension of water at 0 kV is well known in the literature (Kovalchuk, Alberini, and  
112 Simmons 2020; Yousif et al. 2021; Liu and Cao 2021): it is  $72 \text{ mN}\cdot\text{m}^{-1}$ . The measurement of  
113 the ST of a droplet of water was used as a reference measurement in order to compare it to the  
114 measurements made with two other model solutions.

115 The foam-type food matrices can be assimilated to liquid protein solutions in which a gas  
116 injection is performed. The second model solution was an aqueous solution of Whey Protein  
117 Isolate (WPI). WPI is a protein of animal origin, an isolate's short chain proteins that are  
118 extracted from Whey Protein Concentrate also known as WPC, derived from milk. Techno-  
119 physical properties such as ST (Bazinet, Trigui, and Ippersiel 2004), viscosity (Bazinet, Trigui,  
120 and Ippersiel 2004; Wang et al. 2021) or gas solubility (Said et al. 2022) of WPI-based solutions  
121 are available in the literature. This is why we chose to use this first protein solution in order to

122 reconcile our results with existing data. Several works (Laporte, 2014; Nicorescu, 2009;  
123 Talansier et al, 2012) highlighted the difficulty of dissolving WPI in the aqueous phase and  
124 obtaining a homogeneous solution. Based on the work of Talansier et al. (2012), we defined a  
125 protocol specific to our experiment. We decided to prepare solutions containing 3% WPI. The  
126 total mass of WPI was incorporated in 4 times, staggered at 15mn intervals, under moderate  
127 agitation (3-blade propeller, speed 100 rpm), at room temperature (20°C), to guarantee the  
128 complete dissolution of the powder. After complete dissolution of the WPI, the solution was  
129 transferred into the pendant droplet tensiometer.

130 Considering a clean label approach, a protein of plant origin was considered for the third model  
131 solution, namely an aqueous chickpea protein solution (CKP). According to Buhl et al. (2019),  
132 aquafaba has shown good food functional properties, as this plant-based liquid has the ability  
133 to function as both a foaming agent and an emulsifier under conditions of pH and NaCl  
134 concentrations that happen to be those readily encountered in food products. As a vegetable  
135 alternative to egg white or WPI, CKP aquafaba seems to be an interesting candidate for foamed  
136 products. Therefore, we decided to use a chickpea aquafaba-based solution. The aquafaba from  
137 10 cans was collected by sieving. It was then centrifuged to ensure homogeneity of the mixture.  
138 A sample of this aquafaba was taken for determination of the protein content by the Dumas  
139 method (protein content of 3% +/- 0.2%).

140 The distilled water and the WPI and CKP solutions made the 3 model solutions used in this  
141 study, which will imitate the behaviour of gas/liquid interfaces of foam-type food matrices in  
142 the presence of an SEF.

## 143 2.2. Experimental set-up

144 The liquid droplet was generated using a TRACKER™ automatic droplet tensiometer,  
145 manufactured by TECLIS Instruments (formerly IT Concept) and modified to allow a high  
146 voltage generator (Figure 1). The droplet had a volume of ca. 8μL, which was regulated by a  
147 PID system. Volumetric calibration was performed by the software supplied with the  
148 equipment. The observation of the droplet was done with a fast camera (MELLES GRIOT /  
149 CCD / 640x480 / 60 frames per seconds) illuminated by a stroboscopic LED light source (180  
150 lm / ø 45mm). Using a high voltage source (Ottersweier), an electric field was applied to the  
151 droplet using two parallel electrodes (10x45mm / 1mm thick / stainless steel), positioned on  
152 either side of the droplet, in a 3D printed ABS plastic holder (1.25 cm wide square section).

153 The experiment consisted of applying several positive voltage values: 0 kV ; +0.5 kV ; +1 kV  
154 ; +1.5 kV ; +2 kV ; +4 kV ; +6 kV ; +8 kV ; +10 kV. With the geometry of our experimental  
155 set up, this corresponds to an electric field value between 0 to 800 kV/m because the electrodes  
156 gap is 12.5 mm. For the calculation, we neglect the thickness of the glass wall which leads us  
157 to an uncertainty of 5% on the measurement. The SEF was applied for a period of 120 seconds.  
158 The experimental set up generates automatically the drop (about 5 seconds) and then the  
159 recording of surface tension starts. We observed that 120 seconds was enough to reach an  
160 equilibrium state for protein dynamic in the 8 $\mu$ L droplet. At the end of this time, a photo of the  
161 droplet was taken in each case, with or without SEF. Between each voltage value, a photo of  
162 the droplet was taken at 0 kV. The experiment was repeated 5 times for each solution and each  
163 voltage value. Then, the pictures of the droplets were transferred to the ImageJ software in order  
164 to calculate the ST according to the method presented in the following paragraph.

165 In an ideal equilibrium situation (no liquid withdrawal, zero flow rate), the tangential electric  
166 field on the electrified meniscus surface is zero. In the liquid side, the electric field vanishes,  
167 since there are no liquid motions and no need for a compensating electric field (Gañán-Calvo,  
168 Dávila, and Barrero 1997).

169 When the droplet is placed between two flat electrodes, the situation is a bit more complex.  
170 The distribution of electric charges is heterogeneous in the droplet, but is organized  
171 symmetrically on either side of the droplet center. The electrical relaxation time  $t_e = \beta \epsilon_0 / K$   
172 is small compared to the hydrodynamic time  $T_h \sim L/U$ , which is the time required for the fluid  
173 particles with characteristic velocity U to move across a zone of characteristic size L.

174 In that case, the liquid bulk is quasi-neutral and the free charges are confined to a very thin  
175 layer, of the order of Debye's length, underneath the liquid-gas interface (Nath, Borthakur, and  
176 Biswas 2020).

177 From the electrical point of view, the liquid bulk acts as an Ohmic conductor whose electric  
178 conductivity is given by the mobilities of the positive and negative ion species in a quasi neutral  
179 solution (Gañán-Calvo, Dávila, and Barrero 1997).

### 180 [2.3 Apparent surface tension calculation method](#)

181 Among different methods used for the measurement of interfacial tension, the pendant droplet  
182 is particularly well adapted to a liquid – liquid interface (Faour et al. 1996; Gassin 2014). It is  
183 based on the deformation of a droplet depending on the interfacial tension. To describe the

184 shape of interfaces (Figure 2), Young-Laplace introduced an equation that combines the  
 185 curvature of the interface, the ST, and the hydrostatic pressure:

$$186 \quad -\Delta\rho gz + \gamma \frac{2}{R_0} = \gamma \left[ \frac{1}{r_1} + \frac{1}{r_2} \right] \quad (2)$$

187 The most usual method was developed by Rotenberg: from an approximated initial value of  $\gamma$ ,  
 188 Laplace's equation is numerically integrated by successive iterations using the Runge–Kutta  
 189 method until the computed and the digitized profiles coincide (Berry et al. 2015). Using the  
 190 dimensionless coordinates X, Y and S such as  $X = \frac{x}{R_0}$ ,  $Y = \frac{y}{R_0}$ ,  $S = \frac{s}{R_0}$  and using that  $R_1 = \frac{ds}{d\theta}$   
 191 and  $R_2 = \frac{x}{\sin\theta}$  the Young-Laplace equation can be rewritten in the following parametric form  
 192 (Dingle et al. 2005):

$$193 \quad \frac{d\theta}{dS} = 2 - \beta Y - \frac{\sin\theta}{X} \quad (3)$$

$$194 \quad \frac{dX}{dS} = \cos\theta$$

$$195 \quad \frac{dY}{dS} = \sin\theta \quad (4)$$

196 Here we define  $\beta = \frac{\Delta\rho g R_0^2}{\gamma}$

197 To characterize the shape of the droplet, the parameter  $\sigma = \frac{D_e}{D_s}$  was introduced. The use of the  
 198 following polynomial formulas, which are approximations of the Fordham tables, allow to  
 199 deduce from  $\sigma$  an approximate value of the two parameters  $\beta$  and  $R_0$ :

$$200 \quad \beta = 0.12836 - 0.7577\sigma + 1.7713\sigma^2 - 0.5426\sigma^3 \quad (5)$$

$$201 \quad \frac{D_e}{2R_0} = 0.9987 + 0.1987\beta - 0.0734\beta^2 + 0.34708\beta^3 \quad (6)$$

202 Thus, the value of the apparent ST was obtained as follows:

$$203 \quad \gamma = \frac{\Delta\rho g R_0^2}{\beta} \quad (7)$$

204 As the ST is determined from experimental profiles of a droplet, it is considered as an apparent  
 205 interfacial tension (Berry, 2015). The literature (Gassin, 2014) states that the results obtained  
 206 with this method are an approximate value at about 10%. This uncertainty comes mainly from  
 207 the uncertainties on  $\beta$  and  $R_0$  related to their determination, and to the definition of the droplet



208 profile. More precise methods can be used but they require the numerical solution of Maxwell's  
209 equations and a huge computational effort (Dingle et al. 2005).

210 Several authors have been interested in measuring the ST of water as well as WPI and chickpea  
211 aquafaba solutions. They used the pendant drop tensiometer method coupled with image  
212 analysis, and the method that correlates ST to the drop time curves (Ghribi et al. 2015). Table  
213 1 summarizes the different values of the ST of these solutions in the absence of an SEF. As  
214 expected, these data indicate that WPI and CKP considerably reduce the ST. These values are  
215 considered as reference measurements that should validate our methodology.

216 Berry et al. (2015) recall that the Young-Laplace equation can only be solved analytically for  
217 the trivial case where the drop profile is a sphere. As soon as the drop undergoes a geometrical  
218 deformation, the use of the Young-Laplace equation becomes more uncertain, and the equations  
219 must be solved numerically. The use of the Bond number is recommended to confirm the  
220 observations made by measuring the ST. The Bond number ( $Bo$ ) is a dimensionless number  
221 that represents the ratio between the gravitational forces and the ST on an interface between  
222 two fluids:

$$223 \quad Bo = \frac{\Delta\rho g R_0^2}{\gamma} \quad (8)$$

224 With:

- 225 ➤  $\Delta\rho$ , density difference of the two fluids ( $\text{kg/m}^3$ )
- 226 ➤  $R_0$ , characteristic length, here the radius of the drop (m) from its centre (initially  
227 defined when it had a spherical shape) to its edge

### 228 3. RESULTS

229 Figure 3 presents the influence of the SEF on the shape of distilled water, WPI and CKP  
230 solutions droplets generated with the pendant droplet tensiometer.

231 In order to verify that the changes in the geometry of the droplets observed in Figure 3 are  
232 reversible, we recorded an image 10 seconds after the SEF was stopped (Figure 4). With the  
233 example of the CKP, we can see that the droplet returns to its initial shape (i.e. the one it has  
234 when the SEF is not applied).

235 Figure 5 shows the evolution of the surface tension (calculated using the images, some of  
236 which are shown in Figure 4) as a function of the applied electric field.

237 **3.1. Impact of SEF on distilled water droplets**

238 When no voltage was applied across the electrodes, a spherical (Laplacian) droplet was  
239 observed. As the voltage increased, the droplet elongated in the direction of the gravitational  
240 field, in a direction perpendicular to the applied SEF. Siedel et al. (2018) noted an elongation  
241 of the droplets in the same direction as the electrostatic force, but their experimental set-up was  
242 different (electrodes positioned at the top and bottom, not at the side, and generation of gas  
243 bubbles, not liquid). The fact that the droplets exposed deformation perpendicularly to the  
244 applied SEF can be explained by the reduction of the ST at the air/liquid interface (Sato, Kudo,  
245 and Saito 1999): the cohesive forces that interact within the droplet allowing it to maintain its  
246 spherical shape were reduced, the droplet was then more subjected to the gravitational field,  
247 and it deformed in the same direction as that field. As mentioned by Filali, Er-Riani, and El  
248 Jarroudi (2021), the electric field discontinuity across the interface creates a jump of Maxwell's  
249 stress tensor that is similar to an electric pressure. The cohesive forces were so reduced when  
250 high voltages (10 kV) were applied that it became difficult to generate a single droplet at the  
251 tip of the syringe; as a consequence, the droplets detached from the syringe on some occasions.

252 **3.2. Impact of SEF on WPI solution droplet**

253 For WPI and CKP aquafaba solutions, the observations and deductions were similar to those  
254 made with the previous case (distilled water). However, it should be noted that the droplet  
255 deformed more at lower voltages than in the distilled water case. This can be explained by a  
256 cumulative effect due to the presence of the WPI: the proteins have their own surface active  
257 effect (Said et al. 2022), which reduced the ST and came in synergy to the effect of the  
258 electrostatic field. It was not possible to take pictures of droplets at 8 and 10 kV because the  
259 surface voltage was too low to generate a droplet at the tip of the syringe. Either the droplet  
260 remained too short before it broke off to make a clear picture, or a continuous stream of liquid  
261 escaped from the needle.

262 **3.3. Impact of SEF on chickpea aquafaba droplets**

263 It was not possible to obtain images at 8 or 10kV for the same reasons as explained above.  
264 The same effects of SEF on the CKP droplet as with the WPI droplet were observed: elongation  
265 in the direction of the gravitational field, droplet deformed more at lower voltages than in the  
266 distilled water case. According to Figure 5, the ST values for each applied voltage were close  
267 between WPI and CKP, WPI being slightly more surface active than CKP at 0kV. This is in

268 line with the literature (Oo and Soe 2017) which proposes CKP as a vegetable alternative to  
269 WPI.

### 270 3.4. Impact of SEF on the apparent surface tension

271 The Figure 5 shows the evolution of the ST at the air/liquid interface of the droplet as a  
272 function of the electric field strength (applied voltage on the electrode gap). A clear decrease in  
273 apparent ST was observed with increasing voltage: 68% for distilled water, 54% for WPI and  
274 53% for CKP (values for a decrease in ST between 0 and 6 kV). A similar protein content (about  
275 3%) may explain the very similar evolution between WPI and CKP. The slight differences  
276 observed can be explained by the structural differences of the WPI and CKP proteins.

277 These observations are supported by the evolution of the Bond number as a function of the  
278 applied electric field (Figure 7). We observe a decrease of the Bond number with the increase  
279 of the voltage applied to the terminals of the electrodes.  $Bo$  being defined as the ratio between  
280 the gravitational forces and the ST, we can therefore confirm that the ST decreases. Berry et al.  
281 (2015) consider that the pendant droplet tensiometry is a simple method to determine the  
282 interfacial tension, but they warn that the method is inaccurate when the Bond number is low.  
283 They consider that the method is no longer suitable if  $Bo < 0.1$ , which is not our case.

284 In distilled water, molecules undergo very short-range interactions (attractive Van der Waals  
285 interaction). The Van der Waals bond is the electrostatic attraction or repulsion between  
286 molecules with permanent or temporary dipoles. The application of the electric field changes  
287 the dipole moment of the water molecules, which also changes the anisotropy of the molecular  
288 interaction forces, thus decreasing the ST.

289 For solutions containing proteins, this effect is present but the effect of the electric field on the  
290 proteins is also added.

291 The surface-active properties of proteins are due to their amphiphilic structure, which prevents  
292 the immediate recombination of newly created droplets via the Marangoni effect, stabilizes the  
293 formed droplets by decreasing the pressure gradient at the interface, and stabilizes the droplets  
294 against aggregation, by providing electrostatic or steric repulsions between the droplets.

295 As the function of proteins depends directly on their structure, any constraint imposed by the  
296 presence of an electric field can potentially become harmful. Astrakas, Gousias, and Tzaphlidou  
297 (2011) have shown that the electric field induces conformational changes in proteins. In  
298 addition, there is evidence that the electric field accelerates the folding and unfolding rates of

299 globular proteins in solution. For example, exposure to electric and electromagnetic fields may  
300 be considered in the design of alternative treatment strategies for amyloid diseases because of  
301 their inhibitory effect on the conformations of amyloid gene peptides of intermediate strength  
302 (De Pomerai et al. 2003). Some studies on the alterations of protein conformations under the  
303 influence of SEF, show the role of hydrogen bonds. Hydrogen bonds play a fundamental role  
304 in controlling protein activity during enzymatic action—folding, binding with other proteins,  
305 and other processes. Changes in the strength of hydrogen bonds, induced by an electric field,  
306 can affect these processes (Astrakas, Gousias, and Tzaphlidou 2011).

307 Sato et al. (1999) calculated that the ST reduction due to applied voltage was proportional to  
308 the square of the voltage. We also introduce a quantity  $\gamma_E$ , called ST reduction, which is  
309 calculated as follows:

$$310 \qquad \qquad \qquad \gamma_E = \gamma_0 - \gamma \qquad \qquad \qquad (9)$$

311 With:

- 312       ➤  $\gamma_0$ , value of surface tension when no voltage was applied
- 313       ➤  $\gamma$ , value of surface tension at a single value of applied voltage

314 The ST reduction (defined by equation 9) as a function of the voltage applied is plotted in  
315 Figure 6. As shown in the figure, the model proposed by Sato was not adequate in our case  
316 where a power law is suited. This difference is due to the measurement method used by Sato et  
317 al.. They proposed a specific equation to calculate the ST from the theory on vibrating but it  
318 required some correction factors. As previously explained, our calculation method is based on  
319 the traditional Young-Laplace equation, which applies to spherical drops. Bateni, Amirfazli,  
320 and Neumann (2006) performed an error analysis to examine the quality of the Laplacian curve  
321 fittings at high voltages. It was found that the measurements between 1kV to 7 kV are generally  
322 at the same level of reliability as those in the absence of an electric field. The measurements up  
323 to 8 kV were found to be less reliable, possibly because the shape of a drop deviates from the  
324 Laplacian relation, close to the stability limit.

325 According to Mhatre et al. (2019), the classically used Young-Laplace equation could be  
326 modified to include electrostatic effects. When a drop is exposed to an electric field, the shape  
327 of the drop at equilibrium is due to the Maxwell stress at its interface which is balanced by an  
328 interfacial tension force. Starting from the equation (2), they define the modified Young-  
329 Laplace equation in SEF:

330

$$331 \quad \gamma \left( \frac{1}{R_1} + \frac{1}{R_2} \right) = \Delta\rho_0 - \Delta\rho g z + \frac{1}{2} \epsilon \cdot E_n^2 \quad (10)$$

332 Where:

- 333 ➤  $\epsilon$  is permittivity of the medium phase
- 334 ➤  $E_n$  is the normal component of SEF at the drop interface
- 335 ➤ The last term on the right side of the above equation denotes the normal component of
- 336 the Maxwell stress.

337 This additional term is suited for a perfectly conducting drop in a pure dielectric medium.  
338 Mhatre et al. (2019) indicated that as the strength of the SEF increases, the radius of curvature  
339 at the top of the drop decreases, but if the Maxwell stress term is not included in the Young-  
340 Laplace equation, the estimated interfacial tension is misleading and significantly lower than  
341 the real interfacial tension. A further step will consist in developing a specific new algorithm  
342 to evaluate the ST from Eq. 10.

#### 343 4. CONCLUSION & PERSPECTIVES

344 The pioneer investigations presented in this paper aimed at assessing the impact of an external  
345 SEF on the apparent ST of 3 model solutions. It was confirmed that applying an SEF yielded a  
346 significant reduction of the ST of water. Two aqueous protein solutions have been considered  
347 too, also resulting in a significant reduction of the ST under SEF (up to 48%).

348 This decrease in ST can be explained by:

- 349 - A modification of the dipole moments between molecules
- 350 - A modification of the H-bonds and Van der Waals type interactions
- 351 - A change in the conformation of proteins, which then lose their structural properties

352 If the shape of the drop is clearly altered by the SEF, other data treatments should be performed  
353 using the modified Young-Laplace equation. In the search for an innovative process to stabilise  
354 food foams, SEF treatment appears therefore as a promising solution. By reducing the ST, liquid  
355 or gas droplets exposed to SEF are likely to break up more easily under shearing conditions.  
356 Food protein matrices, such as food foams, are even more sensitive to the effect of SEF because  
357 they contain proteins that already have a surfactant effect. By facilitating expansion through the

358 formation of small gas bubbles, SEF reduces the energy consumption required to operate a  
359 mixer and limits the use of surface-active chemicals traditionally used to lower the ST and  
360 stabilise the foam over time. Thus, expansion coupled with SEF offers new horizons in terms  
361 of processing using "clean labelled" foams or emulsions.

## 362 ACKNOWLEDGEMENTS

363  
364 The present paper/communication has been co-funded by ONIRIS-GEPEA and by the  
365 FEDER European funds Ref 2020/FEDER/n°PL0019794 within the international Chair  
366 "CONT-E-FOOD" on continuous food processes under electrical disturbances. Disclaimer: the  
367 content found in this contribution reflects only the author's view. The EU commission is not  
368 responsible for any use that may be made of the information it contains.

369 We thank Pedro Llovera-Segovia (Instituto de Tecnología Eléctrica - Universitat Politècnica  
370 de València, Spain) for his contribution on electrostatic phenomena.

## 371 REFERENCES

- 372 Astrakas, Loukas, Christos Gousias, and Margaret Tzaphlidou. 2011. "Electric Field Effects on  
373 Chignolin Conformation." *Journal of Applied Physics* 109 (9).  
374 <https://doi.org/10.1063/1.3585867>.
- 375 Audebert, Alexia. 2018. "Stabilisation et Texturation de Mousses Liquides Par Des Protéines  
376 de Lactosérum Chauffées à l'état de Poudre." Université Bretagne Loire.  
377 <https://www.theses.fr/2018NSARB317>.
- 378 Bateni, A., A. Amirfazli, and A. W. Neumann. 2006. "Effects of an Electric Field on the Surface  
379 Tension of Conducting Drops." *Colloids and Surfaces A: Physicochemical and*  
380 *Engineering Aspects* 289 (1–3): 25–38. <https://doi.org/10.1016/j.colsurfa.2006.04.016>.
- 381 Bazinet, Laurent, Maher Trigui, and Denis Ippersiel. 2004. "Rheological Behavior of WPI  
382 Dispersion as a Function of PH and Protein Concentration." *Journal of Agricultural and*  
383 *Food Chemistry* 52 (17): 5366–71. <https://doi.org/10.1021/jf049893v>.
- 384 Berry, Joseph D., Michael J. Neeson, Raymond R. Dagastine, Derek Y.C. Chan, and Rico F.  
385 Tabor. 2015. "Measurement of Surface and Interfacial Tension Using Pendant Drop  
386 Tensiometry." *Journal of Colloid and Interface Science* 454: 226–37.  
387 <https://doi.org/10.1016/j.jcis.2015.05.012>.
- 388 Boissonnet, Guillaume. 1998. "Étude de l'écoulement d'une Mousse Aqueuse de

- 389 Décontamination Hydrodynamique.” Université de Montpellier II.
- 390 Bonhomme, Oriane, Li Peng, and Anne Laure Bianco. 2020. “Thermally Enhanced Electro-  
391 Osmosis to Control Foam Stability.” *Physical Review X* 10 (2).  
392 <https://doi.org/10.1103/PhysRevX.10.021015>.
- 393 Borthakur, Manash Pratim, Gautam Biswas, and Dipankar Bandyopadhyay. 2018. “Dynamics  
394 of Drop Formation from Submerged Orifices under the Influence of Electric Field.”  
395 *Physics of Fluids* 30 (12). <https://doi.org/10.1063/1.5063913>.
- 396 Castellanos, Antonio. 1998. “Electrospray and Atomization.” In *Electrohydrodynamics*, 206–  
397 12. Vienna: Springer Vienna. [https://doi.org/10.1007/978-3-7091-2522-9\\_14](https://doi.org/10.1007/978-3-7091-2522-9_14).
- 398 Dingle, Nicole M., Kristianto Tjiptowidjojo, Osman A. Basaran, and Michael T. Harris. 2005.  
399 “A Finite Element Based Algorithm for Determining Interfacial Tension ( $\gamma$ ) from Pendant  
400 Drop Profiles.” *Journal of Colloid and Interface Science* 286 (2): 647–60.  
401 <https://doi.org/10.1016/j.jcis.2005.01.052>.
- 402 Faour, G, M Grimaldi, J Richou, and A Bois. 1996. “Real-Time Pendant Drop Tensiometer  
403 Using Image Processing with Interfacial Area and Interfacial Tension Control  
404 Capabilities.” *Journal of Colloid and Interface Science* 181 (2): 385–92.  
405 <https://doi.org/10.1006/jcis.1996.0395>.
- 406 Felix, Manuel, Inmaculada Martínez, Ana Sayago, and M<sup>a</sup> Ángeles Fernández Recamales.  
407 2021. “Wine Lees: From Waste to O/W Emulsion Stabilizer.” *Innovative Food Science  
408 and Emerging Technologies* 74 (August). <https://doi.org/10.1016/j.ifset.2021.102810>.
- 409 Filali, Youness, Mustapha Er-Riani, and Mustapha El Jarroudi. 2021. “Deformation of a Fluid  
410 Drop Subjected to a Uniform Electric Field.” *Zeitschrift Fur Angewandte Mathematik Und  
411 Physik* 72 (1): 1–18. <https://doi.org/10.1007/s00033-020-01439-w>.
- 412 Gañán-Calvo, A. M., J. Dávila, and A. Barrero. 1997. “Current and Droplet Size in the  
413 Electro spraying of Liquids. Scaling Laws.” *Journal of Aerosol Science* 28 (2): 249–75.  
414 [https://doi.org/10.1016/S0021-8502\(96\)00433-8](https://doi.org/10.1016/S0021-8502(96)00433-8).
- 415 Gassin, Pierre-Marie. 2014. “Mesure de La Tension Superficielle Par La Technique de La  
416 Goutte Pendante.” <https://www.researchgate.net/publication/260963141>.
- 417 Ghribi, Abir Mokni, Ines Maklouf Gafsi, Christophe Blecker, Sabine Danthine, Hamadi Attia,  
418 and Souhail Besbes. 2015. “Effect of Drying Methods on Physico-Chemical and

- 419 Functional Properties of Chickpea Protein Concentrates.” *Journal of Food Engineering*  
420 165: 179–88. <https://doi.org/10.1016/j.jfoodeng.2015.06.021>.
- 421 Kovalchuk, N., F. Alberini, and M. J.H. Simmons. 2020. “Effect of Moderate DC Electric Field  
422 on Formation of Surfactant-Laden Drops.” *Chemical Engineering Research and Design*  
423 157 (6): 133–41. <https://doi.org/10.1016/j.cherd.2020.03.009>.
- 424 Liu, Jianshu, and Yang Cao. 2021. “Experimental Study on the Surface Tension of Magnetized  
425 Water.” *International Communications in Heat and Mass Transfer* 121 (December 2020):  
426 105091. <https://doi.org/10.1016/j.icheatmasstransfer.2020.105091>.
- 427 Mhatre, Sameer, Sébastien Simon, and Johan Sjöblom. 2019. “Methodology to Calculate  
428 Interfacial Tension under Electric Field Using Pendant Drop Profile Analysis.”  
429 *Proceedings of the Royal Society A: Mathematical, Physical and Engineering Sciences*  
430 475 (2225). <https://doi.org/10.1098/rspa.2018.0852>.
- 431 Nath, Binita, Manash Pratim Borthakur, and Gautam Biswas. 2020. “Electric Field Induced  
432 Dynamics of Viscoplastic Droplets in Shear Flow.” *Physics of Fluids* 32 (9).  
433 <https://doi.org/10.1063/5.0021829>.
- 434 Nicorescu, Irina. 2009. “Étude Du Couplage Procédé/Produit Lors De La Production Des  
435 Mousses Par Des Agrégats Protéïques.” Nantes Université. <https://tel.archives-ouvertes.fr/tel-00872696/document>.
- 437 Notz, Patrick K., and Osman A. Basaran. 1999. “Dynamics of Drop Formation in an Electric  
438 Field.” *Journal of Colloid and Interface Science* 213 (1): 218–37.  
439 <https://doi.org/10.1006/jcis.1999.6136>.
- 440 Oo, Zar, and Soe Soe. 2017. “Physico Chemical and Functional Properties of Chickpea Protein  
441 Isolate.” *International Journal of Biological & Pharmaceutical Research* 3 (12): 1–14.
- 442 Pomerai, David I. De, Brette Smith, Adam Dawe, Kate North, Tim Smith, David B. Archer,  
443 Ian R. Duce, Donald Jones, and E. Peter M. Candido. 2003. “Microwave Radiation Can  
444 Alter Protein Conformation without Bulk Heating.” *FEBS Letters* 543 (1–3): 93–97.  
445 [https://doi.org/10.1016/S0014-5793\(03\)00413-7](https://doi.org/10.1016/S0014-5793(03)00413-7).
- 446 Rio, Emmanuelle. 2013. “Stabilité Des Mousses : Quelques Expériences Montrant l’influence  
447 de La Rhéologie de Surface.” <https://tel.archives-ouvertes.fr/tel-00874063>.
- 448 Said, Mohamed Sasi, Mohd Zaidi Jaafar, Shaziera Omar, and Sairoz Norazlan Sharbini. 2022.



449 “Influence of Whey Protein Isolate on CO<sub>2</sub> Foams Stability in Three Different Types of  
450 Crude Oil.” *Case Studies in Chemical and Environmental Engineering* 5 (May).  
451 <https://doi.org/10.1016/j.cscee.2022.100191>.

452 Sato, Masayuki, Naoya Kudo, and Masahiro Saito. 1999. “Surface Tension Reduction of Liquid  
453 by Applied Electric Field Using Vibrating Jet Method.” *IEEE Transactions on Industry*  
454 *Applications*.

455 Schramm, Laurier L. 2006. *Emulsions, Foams and Suspensions. Emulsions, Foams, and*  
456 *Suspensions*. Wiley-VCH Verlag GmbH & Co. KGaA.  
457 <https://doi.org/10.1002/3527606750.fmatter>.

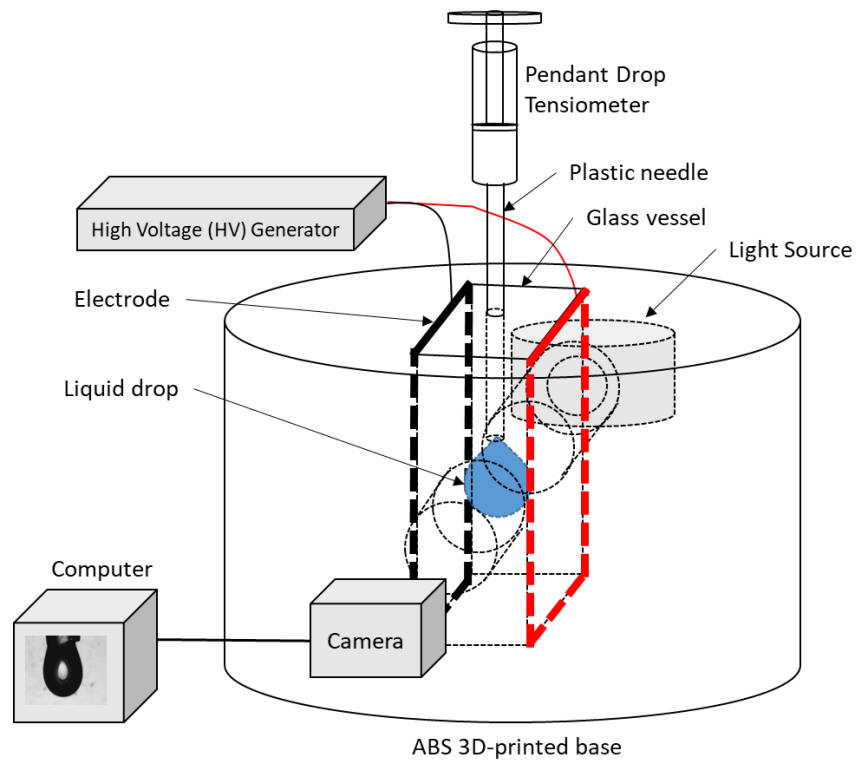
458 Siedel, Samuel. 2012. “Bubble Dynamics and Boiling Heat Transfer: A Study in the Absence  
459 and in the Presence of Electric Field.” *Ph.D. Thesis, Institut National De Sciences*  
460 *Appliquees De Lyon*. <http://theses.insa-lyon.fr/publication/2012ISAL0032/these.pdf>.

461 Wang, Junjing, Morane Jousse, Jitesh Jayakumar, Alejandro Fernández-Arteaga, Silvia de  
462 Lamo-Castellví, Montserrat Ferrando, and Carme Güell. 2021. “Black Soldier Fly  
463 (Hermetia Illucens) Protein Concentrates as a Sustainable Source to Stabilize o/w  
464 Emulsions Produced by a Low-Energy High-Throughput Emulsification Technology.”  
465 *Foods* 10 (5). <https://doi.org/10.3390/foods10051048>.

466 Yousif, Adel M., Richard Snowball, Mario F. D’Antuono, Harmohinder S. Dhammu, and  
467 Darshan L. Sharma. 2021. “Water Droplet Surface Tension Method – An Innovation in  
468 Quantifying Saponin Content in Quinoa Seed.” *Food Chemistry* 343 (May 2020): 128483.  
469 <https://doi.org/10.1016/j.foodchem.2020.128483>.

470

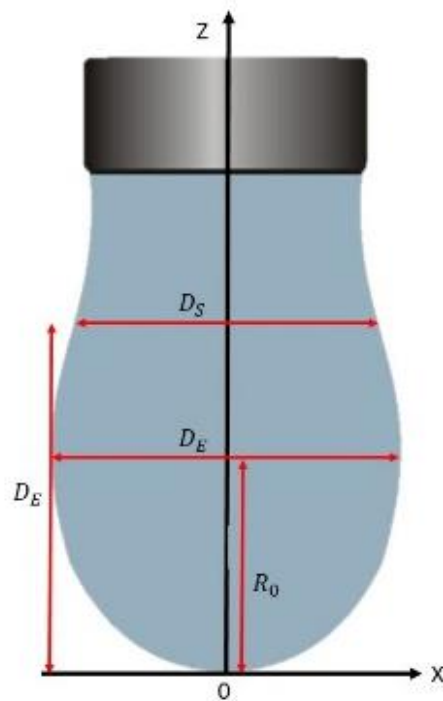
471



472

473

Figure 1 : Pendant droplet tensiometer modified with two parallel electrodes to generate static electric field



474

475

476

Figure 2 : Schema of a pendant droplet with its main geometric dimensions necessary for image analysis

477

Table 1 : Distilled water, 3% WPI solution and Chickpea aquafaba surface tension values at 0kV found in the literature

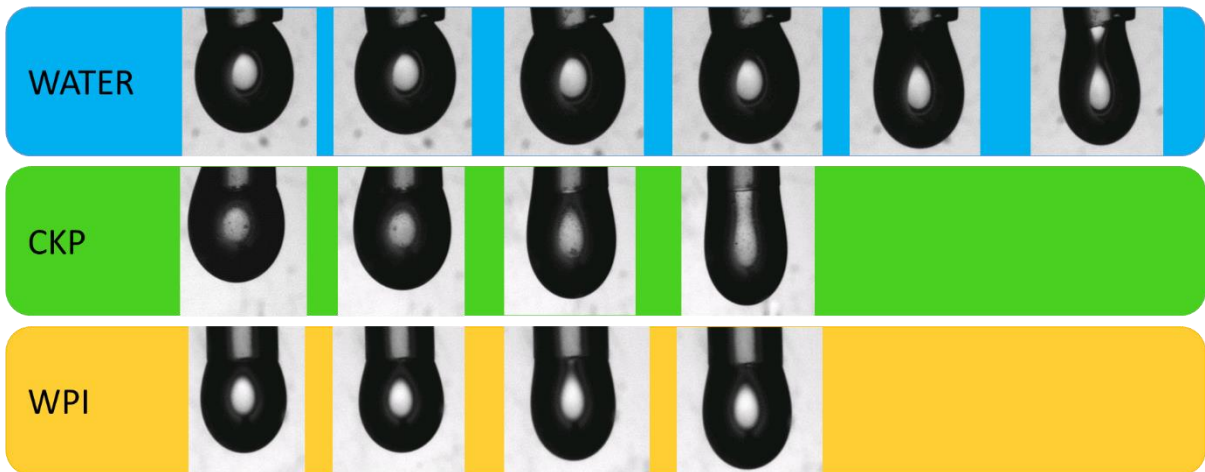
| References            | Surface tension values at 0kV |          |          |
|-----------------------|-------------------------------|----------|----------|
|                       | Distilled water               | WPI (3%) | CKP (3%) |
| Sato et al., 1996     | 72.28                         |          |          |
| Yousif et al., 2020   | 72.15                         |          |          |
| Yadav et al., 2020    | 72                            |          |          |
| Xu et al., 2013       |                               | 49       |          |
| Adhikari et al., 2006 |                               | 42.5     |          |
| Ghribi et al., 2015   |                               |          | 42       |

478

479

480

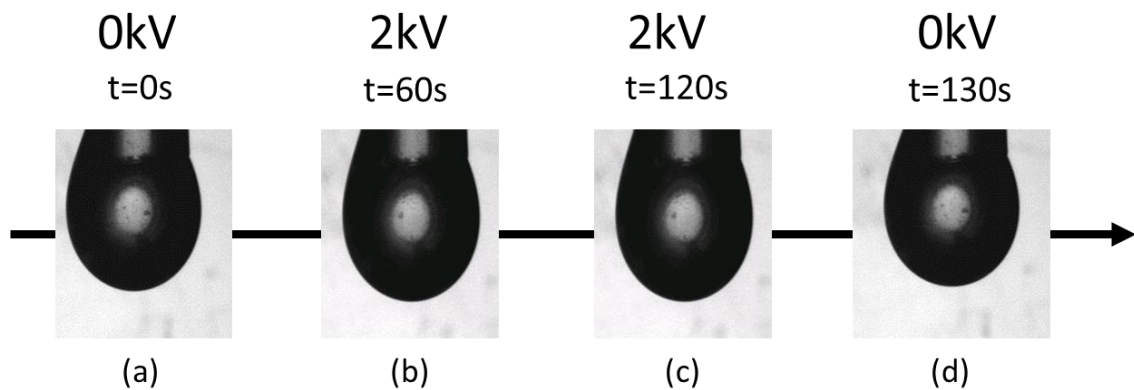
Tension (kV)            0            2            4            6            8            10  
 Electric field (kV/m)    0            160          320          480          640          800



481

482

Figure 3 : Photos of pendant droplets deformed when an electric field is applied at different voltage values



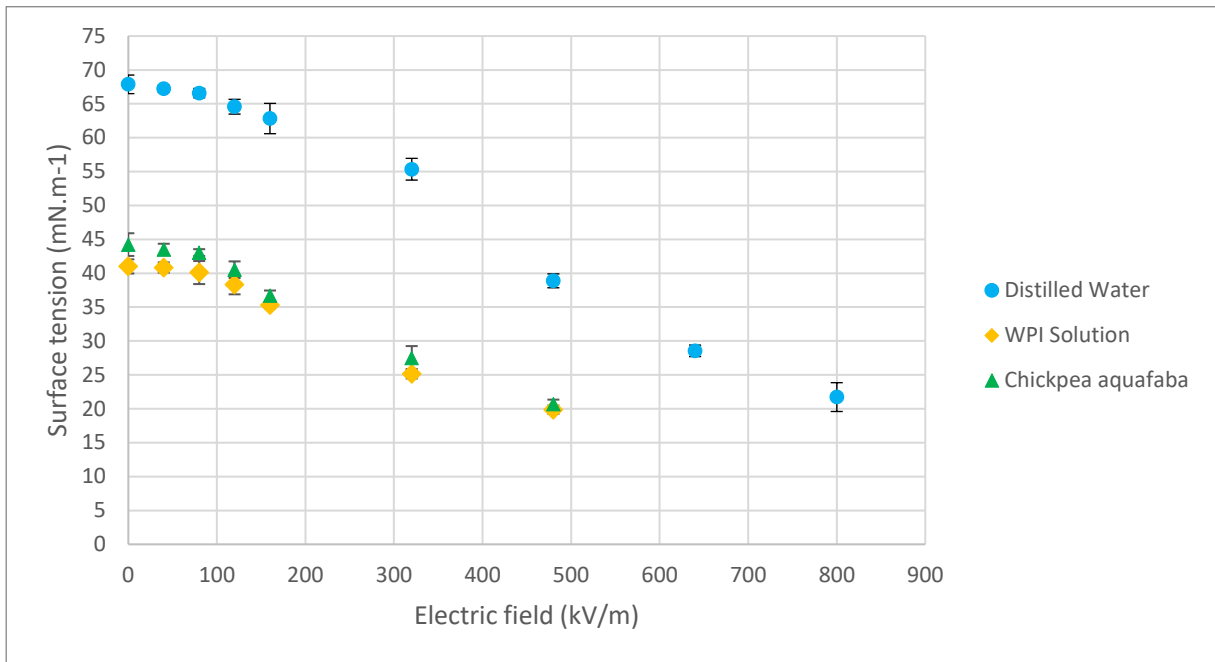
483

484

485

Figure 4 : Photos of CKP pendant droplets during an experiment. (a) Beginning of the experiment (b) Picture at middle of the experiment (c) Photo at the end of the experiment (d) Photo 10s after the end of the experiment

486

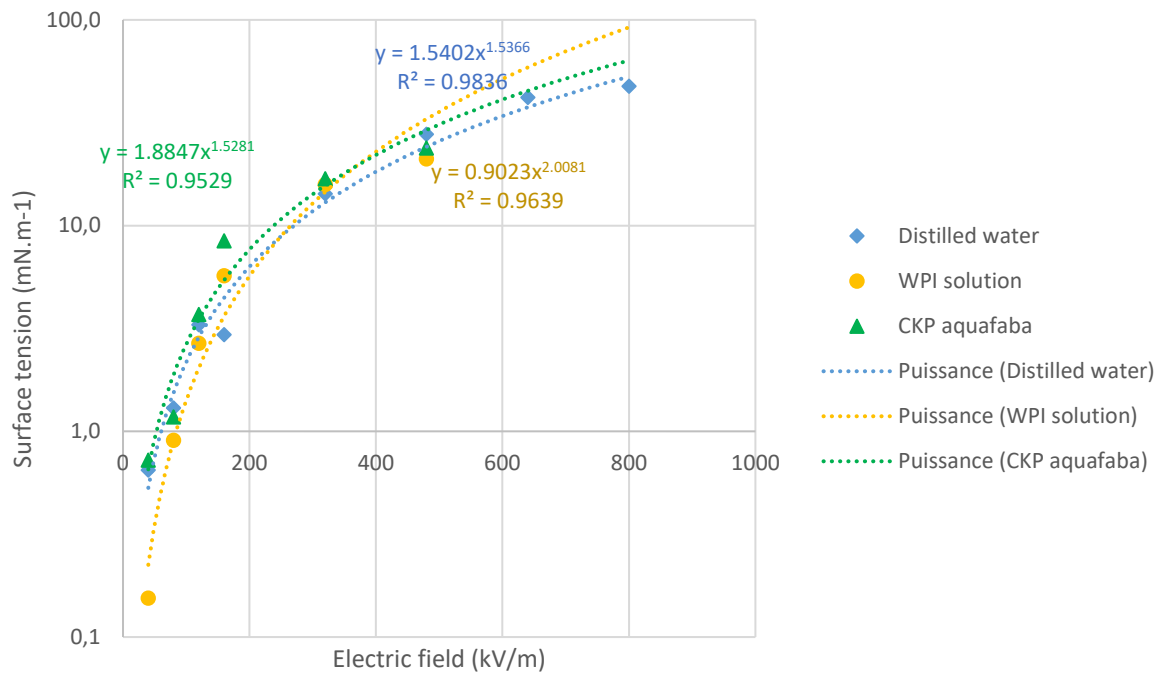


487

488

Figure 5 : Evolution of the surface tension as a function of the electric field applied to the electrodes

489

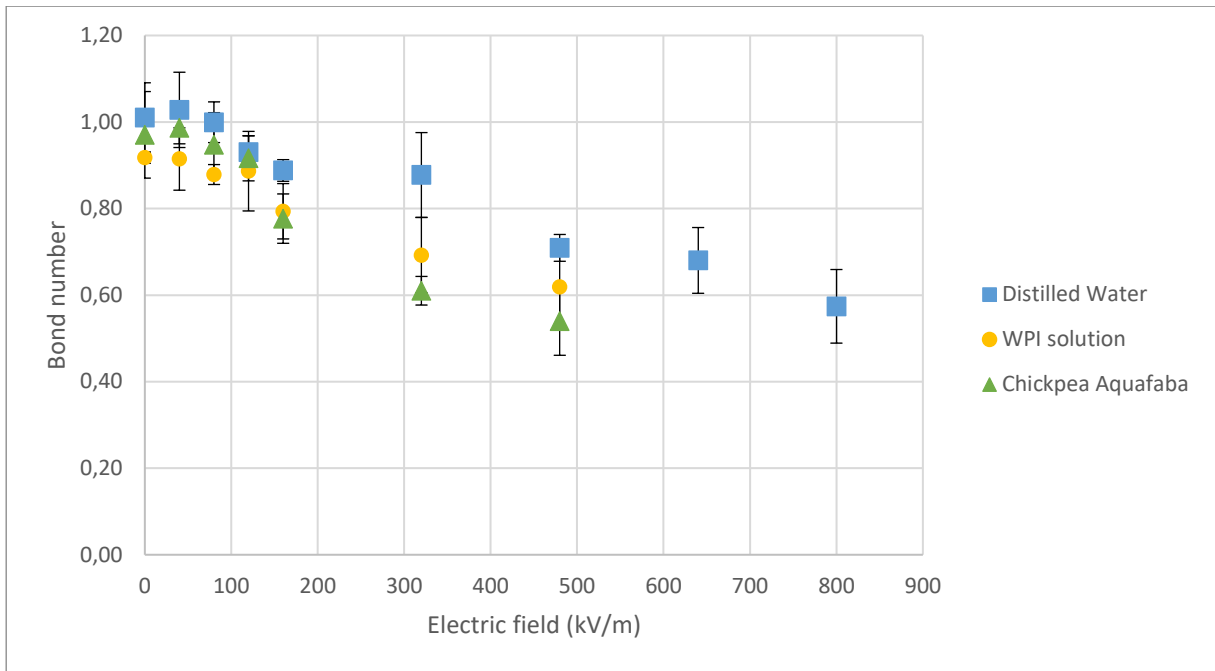


490

491

Figure 6: Surface tension reduction as a function of the electric field applied to the electrode on each side of the pendant drop

492



493

494

Figure 7: Evolution of the Bond number as a function of the electric field applied to the electrodes

495